JACS
JOURNAL OF THE AMERICAN CHEMICAL SOCIETY
Cite This: J. Am. Chem. Soc. 2019, 141, 8047−8052
Communication
pubs.acs.org/JACS

# Direct Observation of Redox Mediator-Assisted Solution-Phase Discharging of Li−$O_2$ Battery by Liquid-Phase Transmission Electron Microscopy

Donghoon Lee,[†,‡,∥] Hyeokjun Park,[†,§,∥] Youngmin Ko,[†,§] Hayoung Park,[†,‡] Taeghwan Hyeon,[†,‡] Kisuk Kang,*[,†,§] and Jungwon Park*[,†,‡]

[†]Center for Nanoparticle Research, Institute for Basic Science, Seoul 08826, Republic of Korea

[‡]School of Chemical and Biological Engineering, Institute of Chemical Processes and [§]Department of Materials Science and Engineering, Research Institute of Advanced Materials, Seoul National University, 1, Gwanak-ro, Gwanak-gu, Seoul 08826, Republic of Korea

Supporting Information



**ABSTRACT:** Li−$O_2$ battery is one of the important next-generation energy storage systems, as it can potentially offer the highest theoretical energy density among battery chemistries reported thus far. However, realization of its high discharge capacity still remains challenging and is hampered by the nature of how the discharge products are formed, causing premature passivation of the air electrode. Redox mediators are exploited to solve this problem, as they can promote the charge transfer from electrodes to the solution phase. The mechanistic understanding of the fundamental electrochemical reaction involving the redox mediators would aid in the further development of Li−$O_2$ batteries along with rational design of new redox mediators. Herein, we attempt to monitor the discharge reaction of a Li−$O_2$ battery in real time by liquid-phase transmission electron microscopy (TEM). Direct in situ TEM observation reveals the gradual growth of toroidal $Li_2O_2$ discharge product in the electrolyte with the redox mediator upon discharge. Moreover, quantitative analyses of the growth profiles elucidate that the growth mechanism involves two steps: dominant lateral growth of $Li_2O_2$ into disclike structures in the early stage followed by vertical growth with morphology transformation into a toroidal structure.

Aprotic Li−air/oxygen (Li−$O_2$) batteries can offer the highest theoretical energy density (~3450 Wh/kg) among the battery systems, because the light and ubiquitous oxygen gas from air is incorporated as a major component.[1] However, a practical Li−$O_2$ battery system has not been demonstrated yet, and many technical and fundamental issues remain to be resolved.[2] One of the issues with respect to the air electrode includes the premature passivation of the electrodes by the discharge products. The initial electrochemical reaction forms an insulating $Li_2O_2$ film on the electrode.[3] It causes the reduction of the electronic conductivity of the electrode and is typically accompanied by undesirable side reactions at the interface between the electrode and $Li_2O_2$. This inevitably leads to a poor energy efficiency and a premature cycle degradation.[4] To mitigate this problem, redox mediators, such as 2,5-di-*tert*-butyl-1,4-benzoquinone (DBBQ), coenzyme Q10, and Vitamin K2, have been recently utilized to induce the discharge process in the solution phase instead of on the electrode.[5] The redox mediators generate stable and soluble intermediate complexes, which catalyze the solution-phase discharge reaction while suppressing the formation of film-like $Li_2O_2$ on the electrode surface.

Mechanistic understanding of relevant chemical reactions in Li−$O_2$ batteries may further provide a rational strategy to optimize cell design, select electrolytes, and engineer electrode materials that can ensure improved energy density with reversible cyclability; however, this has been mainly limited to ex situ information.[6] For example, previous ex situ scanning electron microscopy (SEM) studies could confirm the discharge product of a toroidal $Li_2O_2$ with a relatively large size of a few micrometers, evidencing the solution-phase reaction in the presence of a redox mediator.[6,7] Many mechanistic questions have still remained unanswered such as formation mechanism and kinetic pathway for the observed toroidal $Li_2O_2$ structures and their heterogeneity in different parts of the battery structure. The in situ liquid cell transmission electron microscopy (TEM) of a realistic Li−$O_2$ battery operation can be an appropriate platform to provide decisive information to understand these questions.[8] Herein, we implement a Li−$O_2$ battery system including a discharge redox mediator, DBBQ, and gaseous $O_2$ in the in situ liquid cell TEM and directly observe its discharge process. Our results confirm that the discharge redox mediator promotes two-step formation of $Li_2O_2$ within the solution, which can be attributed to kinetically controlled crystal growth during the electrochemical reaction.

We constructed a micro Li−$O_2$ battery on a liquid cell TEM holder to monitor the discharge process in real time. The Li−$O_2$ microbattery system mimics the bulk battery with a model discharge redox mediator, DBBQ, in $O_2$-saturated electrolytes (Figure 1a). In situ TEM imaging was performed during galvanostatic discharge reaction (Figure 1b). To confirm the reliability of the microbattery system, we compared the cyclic voltammetry (CV) profiles of the microbattery and a bulk cell

**Received:** March 6, 2019
**Published:** May 8, 2019




DOI: 10.1021/jacs.9b02332
J. Am. Chem. Soc. 2019, 141, 8047−8052

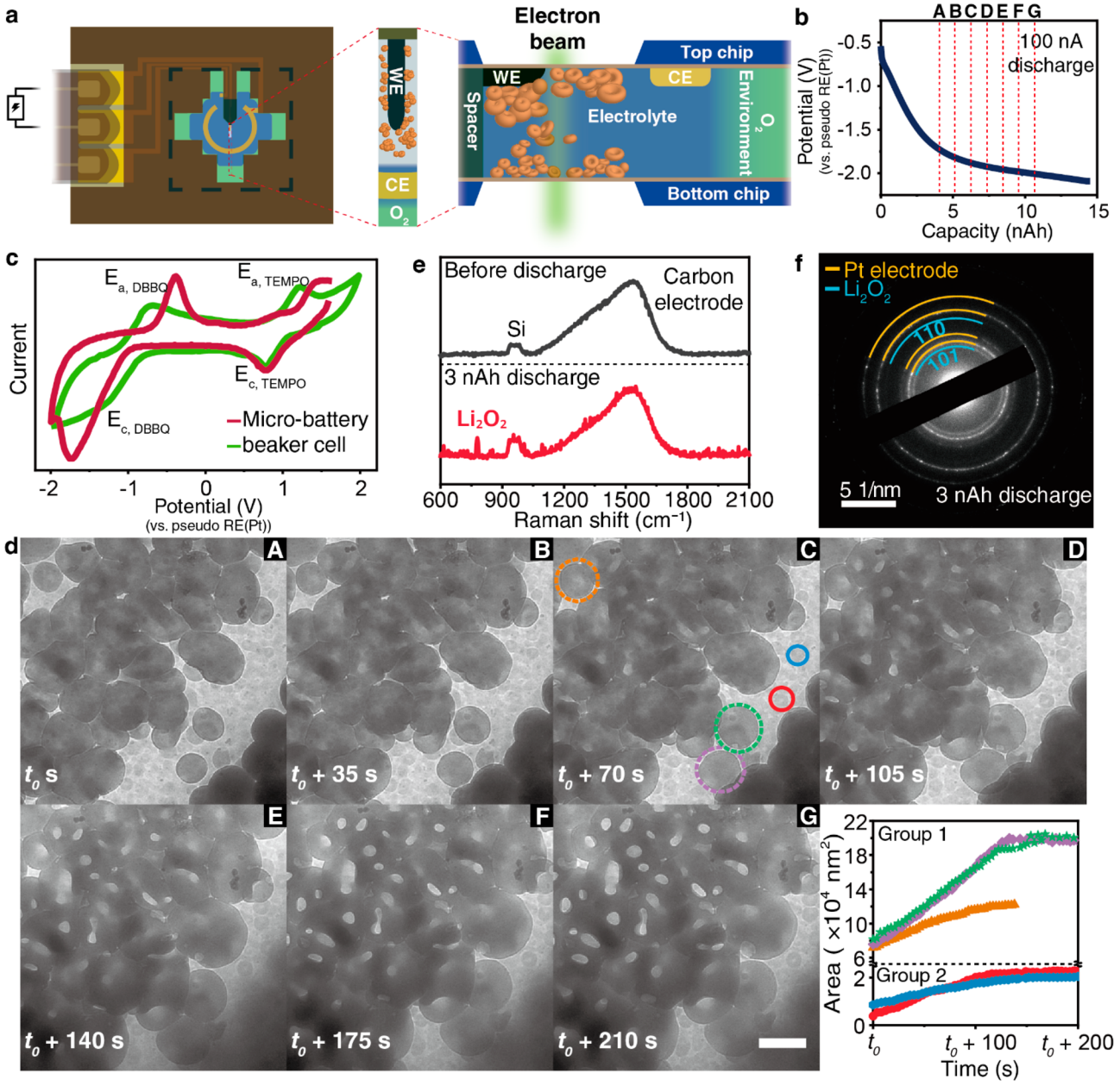


**Figure 1.** (a) Graphical illustration of Li−$O_2$ microbattery in the liquid TEM holder. (b) Galvanostatic voltage profile of the microbattery during discharge. Stages indicated by capital alphabets correspond to TEM images in Figure 1d. (c) CV curves of the microbattery and bulk electrochemical cells containing DBBQ and TEMPO. (d) Time-resolved in situ TEM images of Li−$O_2$ microbattery during discharge. Scale bar is 500 nm. (e) Raman spectra and (f) TEM diffraction pattern of discharge product ($Li_2O_2$). Pt is used as a working electrode (WE) for diffraction measurement to clearly resolve *d*-spacings of $Li_2O_2$.

with the same components as shown in Figure 1c. Note that, in this CV experiment, 2,2,6,6-tetramethyl-1-piperidinyloxy (TEMPO), which is a typical charge redox mediator for Li−$O_2$ batteries, was also added to compare two pairs of redox peaks in the CV curve of the microbattery with those of the bulk cell by estimating the overpotential range.[9] They showed good agreement, which implies that the redox reaction condition in the microbattery system with the redox mediator is a successful reproduction of that in the bulk cell. The details of CV measurement are presented in the Supporting Information.

TEM snapshots from the real-time movie (Movie S1) of the Li−$O_2$ microbattery during discharge process are shown in Figure 1d. The field of view in TEM images in Figure 1d and Movie S1 covers a region filled with electrolyte solution away from the electrode. The series of real-time TEM images in Figure 1d reveal several important features of the discharge reaction in the presence of DBBQ. The formation of $Li_2O_2$ occurs ubiquitously within the electrolyte solution (see Figures S2 and S4 and Section 2 in the Supporting Information). A solid product of the discharge reaction nucleated and grew to a large size in the solution, which was confirmed to be $Li_2O_2$ by ex situ Raman spectroscopy (Figure 1e) and TEM diffraction analysis (Figure 1f). Interestingly, it is observed that several disc-like particles are generated at the beginning and gradually grow to approximately hundreds of nanometers in diameter. Then, the disc-like particles undergo a morphological change rather than growing continuously in the lateral direction. Most


DOI: 10.1021/jacs.9b02332
J. Am. Chem. Soc. 2019, 141, 8047−8052

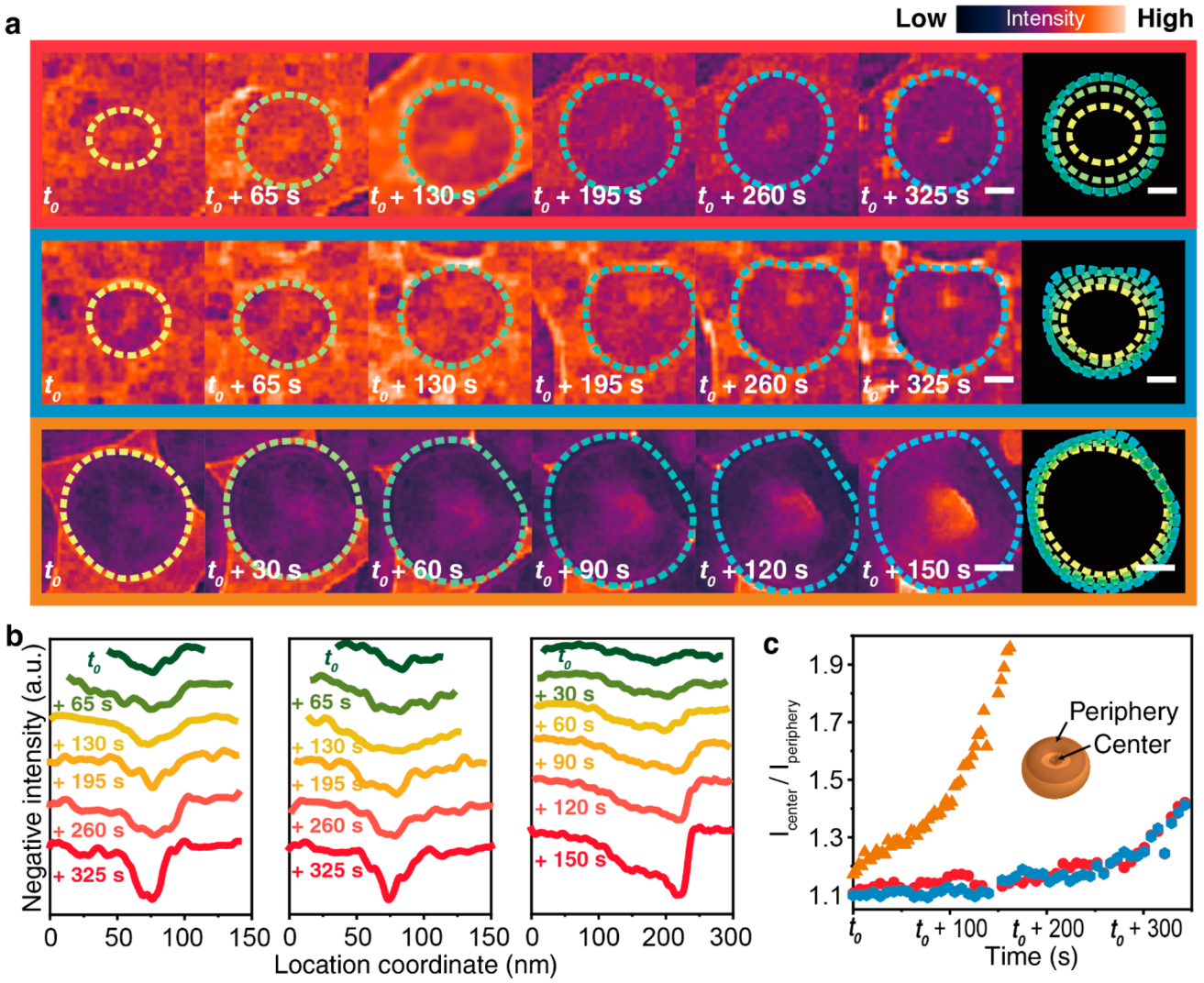


**Figure 2.** (a) Time-resolved TEM images of individual $Li_2O_2$ particles during discharge. From top to bottom, the images are magnified images of particles marked with red, blue, and orange line in Figure 1d, respectively. The overlaid projected areas during discharge are shown in the last image of each row. From top to bottom, the scale bars are 50, 50, and 100 nm, respectively. (b) Line profiles of negative contrast intensity of $Li_2O_2$ particles in Figure 2a (left: red; middle: blue; and right: orange particles, respectively). (c) Center-to-periphery intensity ratio profiles of $Li_2O_2$ particles.

of the particles transform into a specific shape having an asymmetric thickness between their center and periphery while approaching the final stage of the discharge. The formation of unique $Li_2O_2$ particles is not uniform throughout the field of view and rather shows heterogeneity in the rates of nucleation and growth at different places. The growth rates of several $Li_2O_2$ particles were measured (Figures 1d and S3). The particles marked with orange, green, and violet dashed lines (group 1) in Figure 1d grew to a larger size than the particles marked with blue and red solid lines (group 2). The size difference in the last stage of the discharge is ~3 times. The growth of the group 1 is presumably faster, because they are closer to the cathode on the top chip. On the other hand, the particles of the group 2 grow near the bottom chip, which is a few micrometers away from the cathode because of the thickness of the spacer (500 nm) and the window bulging effect.[10] It implies that the diffusion rate of reduced redox mediators can influence the growth rate of the discharge products. Regardless of their different growth kinetics and final sizes, the particles tend to show similar behaviors; that is, the size of the particles converges to a certain value and maintains it.

More details of the growth mechanism of $Li_2O_2$ during discharge can be found from the time-series TEM images of the individual particles shown in Figures 2a and S4, which elucidate the relationship between the growth kinetics and their unique morphological transformation. The time-series TEM images of each particle indicated by different colors in Figure 1d clearly show that the morphology of $Li_2O_2$ changes from disc to toroid during growth. The overlaid projected area of each growing particle (Figure 2a) confirms that the growth in the lateral direction slow down over time and eventually approaches a steady state. The time-resolved line profiles of the individual particles shown in Figure 2b present changes of relative thickness differences between the core and periphery regions of the particles. The details of the line profile measurement are presented in the Supporting Information. The particles shown in Figure 2a have a well-aligned zone axis of ⟨001⟩ direction, an appropriate orientation showing morphology changes. The increasing difference in the contrast



DOI: 10.1021/jacs.9b02332
J. Am. Chem. Soc. 2019, 141, 8047−8052

intensity between the center and periphery with the progress in the discharge process implies that $Li_2O_2$ transforms from disc shape to a toroidal morphology.[11] Three-dimensional intensity maps of the particles during discharge are also plotted, which support this finding (see Figure S6 in the Supporting Information and Movies S2–S4). We also measured the ratio of integrated contrast intensity over the central region to that along the peripheral region, called the areal intensity ratio, of the individual $Li_2O_2$ particles, which are plotted in Figure 2c. Each colored profile corresponds to the particle in Figure 2a marked with the same color. The areal intensity ratio shows a marginal change during initial discharge and indicates that the thickness at the center of the particles is almost the same as that at the periphery. As the discharge proceeds, the areal intensity ratio increases, implying that the thickness along the periphery is larger than that of the center. Furthermore, the increase in areal intensity ratio becomes more rapid after a certain point during the discharge. This indicates that the evolution of the toroidal shape is not continuous but rather composed of two consecutive stages: an initial lateral growth of disclike shape and a subsequent vertical growth of toroidal morphology. We additionally confirm the evolution of toroidal morphology of the $Li_2O_2$ particles by ex situ SEM studies. Bulk $Li–O_2$ cells constructed with typical Swagelok-type systems as explained in Section 1 in Supporting Information were operated with different discharge capacities. While the final toroidal morphology of $Li_2O_2$ after the completion of discharge agrees with the previous ex situ microscopy studies,[7,11,12] it was found that significant morphological changes are clearly accompanied by different discharge capacities (Figure 3). These observations also support the unique two-step formation mechanism of the toroidal morphology of $Li_2O_2$ in the presence of DBBQ.

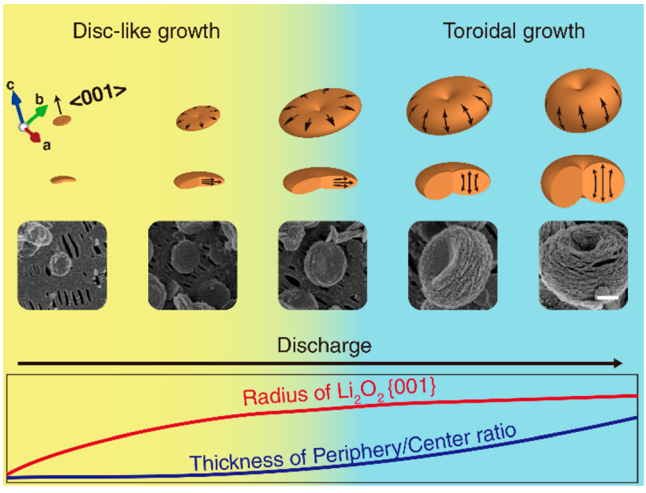


**Figure 3.** Proposed two-step mechanism of solution-mediated $Li_2O_2$ growth processes from the discharge of $Li–O_2$ battery in the presence of DBBQ. (insets) SEM images of $Li_2O_2$ in different cell capacities. Scale bar is 200 nm.

According to the crystallographic structure of $Li_2O_2$, the direction orthogonal to the concave surface in the center of the toroidal $Li_2O_2$ is ⟨001⟩.[12b,13] $Li_2O_2$ particles mainly grow toward lateral directions that are perpendicular to the ⟨001⟩ direction to form a disc shape in the early stage and then toward the ⟨001⟩ direction mainly in the regions along the periphery. This two-step pathway is illustrated in Figure 3 and can be explained by the temperature-dependent surface energy (see Section 3 in Supporting Information). Different from the Wulff construction observed at high temperature in which formation of hexagonal $Li_2O_2$ occurred,[14] the morphology of the $Li_2O_2$ in typical $Li–O_2$ batteries operated at room temperature follows toroidal shape. The step energy, which is in the order of tens of milli-electronvolts per angström for $Li_2O_2$ at room temperature,[15] becomes significant at low temperature. Also, the diffusivity of reaction species including oxygen in the electrolyte at room temperature is relatively low.[16] In this scenario, it is likely that the growth of $Li_2O_2$ particles during discharge is kinetically controlled. In the early stage of discharge, $Li_2O_2$ particles grow at a faster rate in the lateral direction than in the vertical direction, since the total surface energy of the facets parallel to the ⟨001⟩ directions is greater than that of the {001} plane according to previous theoretical studies.[14b,17] As the particles grow at room temperature and in low oxygen diffusive condition, ledges and kinks can form easily around the peripheral edges with high frequency. The growth rate toward the lateral direction accelerates further due to the increased divergence of the surface energy by the continuous generation of surface defects. As a result, the peripheral region of $Li_2O_2$ particles grows thicker than the central part.

In summary, we investigated a $Li–O_2$ microbattery by in situ liquid phase TEM and directly observed that $Li_2O_2$ particles form in the solution in the presence of DBBQ during the discharge process via a two-step pathway involving lateral growth forming disclike particles followed by vertical growth mainly along the peripheral region forming a toroidal morphology. The growth rate of $Li_2O_2$ depends on the distance from the cathode where the DBBQ is reduced. As the use of oxygen evolution reaction (OER) redox mediators becomes standard approach for $Li–O_2$ battery containing oxygen reduction reaction (ORR) redox mediators,[18] we envision that further in situ liquid TEM study can provide direct observations for mechanistic understanding of complex $Li–O_2$ battery chemistry.

## ■ ASSOCIATED CONTENT

### Supporting Information

The Supporting Information is available free of charge on the ACS Publications website at DOI: 10.1021/jacs.9b02332.

Experimental details, description of redox mediators and statistical description for the morphology of $Li_2O_2$, and figures (PDF)
Real-time TEM movie (AVI)
Real-time TEM movie (AVI)
Real-time TEM movie (AVI)
Real-time TEM movie (AVI)

## ■ AUTHOR INFORMATION

### Corresponding Authors

*matlgen1@snu.ac.kr (K.K.)
*jungwonpark@snu.ac.kr (J.P.)

### ORCID

Taeghwan Hyeon: 0000-0001-5959-6257
Kisuk Kang: 0000-0002-8696-1886
Jungwon Park: 0000-0003-2927-4331

### Author Contributions

‖These authors contributed equally.



DOI: 10.1021/jacs.9b02332
J. Am. Chem. Soc. 2019, 141, 8047–8052

### Notes

The authors declare no competing financial interest.

## ■ ACKNOWLEDGMENTS

This work was supported by IBS-R006-D1, the National Research Foundation (NRF) of Korea, funded by the Korea government (MSIT) (No. NRF-2017R1C1B2010434 and NRF-2017R1A5A1015365), the Ministry of Trade, Industry & Energy and Korea Semiconductor Research Consortium support program for the development of future semiconductor devices (No. 10080657), and LG Chem Open Innovation Fund. H. Park, Y. Ko, and K. Kang also acknowledge to the support of IBS-R006-A2 and the NRF grant funded by the Korea government (MSIP) (No. 2018R1A2A1A05079249).

## ■ REFERENCES

(1) (a) Abraham, K. M.; Jiang, Z. A Polymer Electrolyte-Based Rechargeable Lithium/Oxygen Battery. *J. Electrochem. Soc.* **1996**, *143*, 1. (b) Bruce, P. G.; Freunberger, S. A.; Hardwick, L. J.; Tarascon, J. M. Li-$O_2$ and Li-S Batteries with High Energy Storage. *Nat. Mater.* **2012**, *11*, 19. (c) Lee, J.; Kitchaev, D. A.; Kwon, D.-H.; Lee, C.-W.; Papp, J. K.; Liu, Y.-S.; Lun, Z.; Clement, R. J.; McCloskey, B. D.; Guo, J.; Balasubramanian, M.; Ceder, G.; et al. Reversible $Mn^{2+}/Mn^{4+}$ Double Redox in Lithium-excess Cathode Materials. *Nature* **2018**, *556*, 185. (d) Kang, K.; Meng, Y. S.; Breger, J.; Grey, C. P.; Ceder, G. Electrodes with High Power and High Capacity for Rechargeable Lithium Batteries. *Science* **2006**, *311*, 977.

(2) (a) Trahey, L.; Karan, N. K.; Chan, M. K. Y.; Lu, J.; Ren, Y.; Greeley, J.; Balasubramanian, M.; Burrell, A. K.; Curtiss, L. A.; Thackeray, M. M. Synthesis, Characterization, and Structural Modeling of High-Capacity, Dual Functioning $MnO_2$ Electrode/Electrocatalysts for Li-$O_2$ Cells. *Adv. Energy Mater.* **2013**, *3*, 75. (b) Aurbach, D.; McCloskey, B. D.; Nazar, L. F.; Bruce, P. G. Advances in Understanding Mechanisms Underpinning Lithium−Air Batteries. *Nat. Energy* **2016**, *1*, 16128. (c) Lim, H.-D.; Lee, B.; Bae, Y.; Park, H.; Ko, Y.; Kim, H.; Kim, J.; Kang, K. Reaction Chemistry in Rechargeable Li−$O_2$ Batteries. *Chem. Soc. Rev.* **2017**, *46*, 2873. (d) Lyu, Z.; Zhou, Y.; Dai, W.; Cui, X.; Lai, M.; Wang, L.; Huo, F.; Huang, W.; Hu, Z.; Chen, W. Recent Advances in Understanding of the Mechanism and Control of $Li_2O_2$ Formation in Aprotic Li-$O_2$ Batteries. *Chem. Soc. Rev.* **2017**, *46*, 6046.

(3) Wang, J.; Zhang, Y.; Guo, L.; Wang, E.; Peng, Z. Identifying Reactive Sites and Transport Limitations of Oxygen Reactions in Aprotic Lithium-$O_2$ Batteries at the Stage of Sudden Death. *Angew. Chem., Int. Ed.* **2016**, *55*, 5201.

(4) (a) Ottakam Thotiyl, M. M.; Freunberger, S. A.; Peng, Z.; Bruce, P. G. The Carbon Electrode in Nonaqueous Li-$O_2$ cells. *J. Am. Chem. Soc.* **2013**, *135*, 494. (b) Wandt, J.; Jakes, P.; Granwehr, J.; Gasteiger, H. A.; Eichel, R. A. Singlet Oxygen Formation during the Charging Process of an Aprotic Lithium−Oxygen battery. *Angew. Chem.* **2016**, *128*, 7006. (c) Mahne, N.; Schafzahl, B.; Leypold, C.; Leypold, M.; Grumm, S.; Leitgeb, A.; Strohmeier, G. A.; Wilkening, M.; Fontaine, O.; Kramer, D.; et al. Singlet Oxygen Generation as a Major Cause for Parasitic Reactions during Cycling of Aprotic Lithium−Oxygen Batteries. *Nat. Energy* **2017**, *2*, 17036.

(5) (a) Gao, X.; Chen, Y.; Johnson, L.; Bruce, P. G. Promoting Solution Phase Discharge in Li-$O_2$ Batteries Containing Weakly Solvating Electrolyte Solutions. *Nat. Mater.* **2016**, *15*, 882. (b) Liu, T.; Frith, J. T.; Kim, G.; Kerber, R. N.; Dubouis, N.; Shao, Y.; Liu, Z.; Magusin, P.; Casford, M. T. L.; Garcia-Araez, N.; Grey, C. P. The Effect of Water on Quinone Redox Mediators in Nonaqueous Li-$O_2$ Batteries. *J. Am. Chem. Soc.* **2018**, *140*, 1428. (c) Zhang, Y.; Wang, L.; Zhang, X.; Guo, L.; Wang, Y.; Peng, Z. High-Capacity and High-Rate Discharging of a Coenzyme Q10 -Catalyzed Li-$O_2$ Battery. *Adv. Mater.* **2018**, *30*, 1705571. (d) Ko, Y.; Park, H.; Kim, J.; Lim, H.-D.; Lee, B.; Kwon, G.; Lee, S.; Bae, Y.; Park, S. K.; Kang, K. Biological Redox Mediation in Electron Transport Chain of Bacteria for Oxygen Reduction Reaction Catalysts in Lithium−Oxygen Batteries. *Adv. Funct. Mater.* **2019**, *29*, 1805623.

(6) (a) Adams, B. D.; Radtke, C.; Black, R.; Trudeau, M. L.; Zaghib, K.; Nazar, L. F. Current Density Dependence of Peroxide Formation in the Li−$O_2$ Battery and its Effect on Charge. *Energy Environ. Sci.* **2013**, *6*, 1772. (b) Johnson, L.; Li, C.; Liu, Z.; Chen, Y.; Freunberger, S. A.; Ashok, P. C.; Praveen, B. B.; Dholakia, K.; Tarascon, J. M.; Bruce, P. G. The Role of $LiO_2$ Solubility in $O_2$ Reduction in Aprotic Solvents and its Consequences for Li-$O_2$ Batteries. *Nat. Chem.* **2014**, *6*, 1091. (c) Shapiro, D. A.; Yu, Y. S.; Tyliszczak, T.; Cabana, J.; Celestre, R.; Chao, W.; Kaznatcheev, K.; Kilcoyne, A. L. D.; Maia, F.; Marchesini, S.; Meng, Y. S.; Warwick, T.; Yang, L. L.; Padmore, H. A. Chemical Composition Mapping with Nanometre Resolution by Soft X-ray Microscopy. *Nat. Photonics* **2014**, *8*, 765.

(7) (a) Aetukuri, N. B.; McCloskey, B. D.; Garcia, J. M.; Krupp, L. E.; Viswanathan, V.; Luntz, A. C. Solvating Additives Drive Solution-Mediated Electrochemistry and Enhance Toroid Growth in Non-aqueous Li-$O_2$ Batteries. *Nat. Chem.* **2015**, *7*, 50. (b) Burke, C. M.; Pande, V.; Khetan, A.; Viswanathan, V.; McCloskey, B. D. Enhancing Electrochemical Intermediate Solvation through Electrolyte Anion Selection to Increase Nonaqueous Li-$O_2$ Battery Capacity. *Proc. Natl. Acad. Sci. U. S. A.* **2015**, *112*, 9293.

(8) (a) Kim, B. H.; Yang, J.; Lee, D.; Choi, B. K.; Hyeon, T.; Park, J. Liquid-Phase Transmission Electron Microscopy for Studying Colloidal Inorganic Nanoparticles. *Adv. Mater.* **2018**, *30*, 1703316. (b) Lee, W. C.; Kim, B. H.; Choi, S.; Takeuchi, S.; Park, J. Liquid Cell Electron Microscopy of Nanoparticle Self-Assembly Driven by Solvent Drying. *J. Phys. Chem. Lett.* **2017**, *8*, 647. (c) Yang, J.; Koo, J.; Kim, S.; Jeon, S.; Choi, B. K.; Kwon, S.; Kim, J.; Kim, B. H.; Lee, W. C.; Lee, W. B.; Lee, H.; Hyeon, T.; Ercius, P.; Park, J. Amorphous-Phase-Mediated Crystallization of Ni Nanocrystals Revealed by High-Resolution Liquid-Phase Electron Microscopy. *J. Am. Chem. Soc.* **2019**, *141*, 763. (d) Kim, J.; Ou, Z.; Jones, M. R.; Song, X.; Chen, Q. Imaging the Polymerization of Multivalent Nanoparticles in Solution. *Nat. Commun.* **2017**, *8*, 761. (e) Ye, X.; Jones, M. R.; Frechette, L. B.; Chen, Q.; Powers, A. S.; Ercius, P.; Dunn, G.; Rotskoff, G. M.; Nguyen, S. C.; Adiga, V. P.; Zettl, A.; Rabani, E.; Geissler, P. L.; Alivisatos, A. P. Single-Particle Mapping of Nonequilibrium Nanocrystal Transformations. *Science* **2016**, *354*, 874. (f) Baldi, A.; Narayan, T. C.; Koh, A. L.; Dionne, J. A. In situ Detection of Hydrogen-Induced Phase Transitions in Individual Palladium Nanocrystals. *Nat. Mater.* **2014**, *13*, 1143. (g) Zhu, C.; Liang, S.; Song, E.; Zhou, Y.; Wang, W.; Shan, F.; Shi, Y.; Hao, C.; Yin, K.; Zhang, T.; Liu, J.; Zheng, H.; Sun, L. In-situ Liquid Cell Transmission Electron Microscopy Investigation on Oriented Attachment of Gold Nanoparticles. *Nat. Commun.* **2018**, *9*, 421.

(9) Bergner, B. J.; Schurmann, A.; Peppler, K.; Garsuch, A.; Janek, J. TEMPO: a Mobile Catalyst for Rechargeable Li-$O_2$ Batteries. *J. Am. Chem. Soc.* **2014**, *136*, 15054.

(10) Zhu, S.-E.; Krishna Ghatkesar, M.; Zhang, C.; Janssen, G. C. A. M. Graphene Based Piezoresistive Pressure Sensor. *Appl. Phys. Lett.* **2013**, *102*, 161904.

(11) Mitchell, R. R.; Gallant, B. M.; Shao-Horn, Y.; Thompson, C. V. Mechanisms of Morphological Evolution of $Li_2O_2$ Particles during Electrochemical Growth. *J. Phys. Chem. Lett.* **2013**, *4*, 1060.

(12) (a) Gallant, B. M.; Kwabi, D. G.; Mitchell, R. R.; Zhou, J.; Thompson, C. V.; Shao-Horn, Y. Influence of $Li_2O_2$ Morphology on Oxygen Reduction and Evolution Kinetics in Li−$O_2$ Batteries. *Energy Environ. Sci.* **2013**, *6*, 2518. (b) Xia, C.; Waletzko, M.; Chen, L.; Peppler, K.; Klar, P. J.; Janek, J. Evolution of $Li_2O_2$ Growth and Its Effect on Kinetics of Li−$O_2$ Batteries. *ACS Appl. Mater. Interfaces* **2014**, *6*, 12083.

(13) (a) Lim, H.; Yilmaz, E.; Byon, H. R. Real-Time XRD Studies of Li−$O_2$ Electrochemical Reaction in Nonaqueous Lithium−Oxygen Battery. *J. Phys. Chem. Lett.* **2012**, *3*, 3210. (b) Liu, C.; Brant, W. R.; Younesi, R.; Dong, Y.; Edström, K.; Gustafsson, T.; Zhu, J. Towards an Understanding of $Li_2O_2$ Evolution in Li−$O_2$ Batteries: An In Operando Synchrotron X-ray Diffraction Study. *ChemSusChem* **2017**, *10*, 1592. (c) Song, C.; Ito, K.; Sakata, O.; Kubo, Y. Operando



DOI: 10.1021/jacs.9b02332
*J. Am. Chem. Soc.* 2019, 141, 8047−8052

Structural Study of Non-aqueous Li−Air Batteries Using Synchrotron-based X-ray Diffraction. *RSC Adv.* **2018**, *8*, 26293. (d) Ganapathy, S.; Adams, B. D.; Stenou, G.; Anastasaki, M. S.; Goubitz, K.; Miao, X. F.; Nazar, L. F.; Wagemaker, M. Nature of $Li_2O_2$ Oxidation in a Li-$O_2$ Battery Revealed by Operando X-ray Diffraction. *J. Am. Chem. Soc.* **2014**, *136*, 16335. (e) Li, Z.; Ganapathy, S.; Xu, Y.; Heringa, J. R.; Zhu, Q.; Chen, W.; Wagemaker, M. Understanding the Electrochemical Formation and Decomposition of $Li_2O_2$ and LiOH with Operando X-ray Diffraction. *Chem. Mater.* **2017**, *29*, 1577.

(14) (a) Radin, M. D.; Rodriguez, J. F.; Tian, F.; Siegel, D. J. Lithium Peroxide Surfaces are Metallic, While Lithium Oxide Surfaces are Not. *J. Am. Chem. Soc.* **2012**, *134*, 1093. (b) Lee, B.; Kim, J.; Yoon, G.; Lim, H.-D.; Choi, I.-S.; Kang, K. Theoretical Evidence for Low Charging Overpotentials of Superoxide Discharge Products in Metal−Oxygen Batteries. *Chem. Mater.* **2015**, *27*, 8406. (c) Giordani, V.; Tozier, D.; Tan, H.; Burke, C. M.; Gallant, B. M.; Uddin, J.; Greer, J. R.; McCloskey, B. D.; Chase, G. V.; Addison, D. A Molten Salt Lithium-Oxygen Battery. *J. Am. Chem. Soc.* **2016**, *138*, 2656. (d) Xia, C.; Kwok, C. Y.; Nazar, L. F. A High-Energy-Density Lithium-Oxygen Battery based on a Reversible Four-Electron Conversion to Lithium Oxide. *Science* **2018**, *361*, 777.

(15) Hummelshoj, J. S.; Luntz, A. C.; Norskov, J. K. Theoretical Evidence for Low Kinetic Overpotentials in Li-$O_2$ Electrochemistry. *J. Chem. Phys.* **2013**, *138*, 034703.

(16) Schürmann, A.; Haas, R.; Murat, M.; Kuritz, N.; Balaish, M.; Ein-Eli, Y.; Janek, J.; Natan, A.; Schröder, D. Diffusivity and Solubility of Oxygen in Solvents for Metal/Oxygen Batteries: A Combined Theoretical and Experimental Study. *J. Electrochem. Soc.* **2018**, *165*, A3095.

(17) Lee, B.; Seo, D.-H.; Lim, H.-D.; Park, I.; Park, K.-Y.; Kim, J.; Kang, K. First-Principles Study of the Reaction Mechanism in Sodium−Oxygen Batteries. *Chem. Mater.* **2014**, *26*, 1048.

(18) Gao, X.; Chen, U.; Johnson, L. R.; Jovanov, Z. P.; Bruce, P. G. A Rechargeable Lithium-Oxygen Battery with Dual Mediators Stabilizing the Carbon Cathode. *Nat. Energy* **2017**, *2*, 17118.



DOI: 10.1021/jacs.9b02332
*J. Am. Chem. Soc.* 2019, 141, 8047−8052